ELSEVIER

Antimycobacterial activity of new 3-substituted 5-(pyridin-4-yl)-3*H*-1,3,4-oxadiazol-2-one and 2-thione derivatives. Preliminary molecular modeling investigations[☆]

Maria Grazia Mamolo,[a,*] Daniele Zampieri,[a] Luciano Vio,[a] Maurizio Fermeglia,[b] Marco Ferrone,[b] Sabrina Pricl,[b] Giuditta Scialino[c] and Elena Banfi[c]

[a]*Department of Pharmaceutical Sciences, Piazzale Europa 1, University of Trieste, 34127 Trieste, Italy*
[b]*Department of Chemical, Environmental and Raw Materials Engineering, Piazzale Europa 1, University of Trieste, 34127 Trieste, Italy*
[c]*Department of Biomedical Sciences, Microbiology Section, Via A. Fleming 32, University of Trieste, 34127 Trieste, Italy*

Abstract—3*H*-1,3,4-Oxadiazole-2-thione and 3*H*-1,3,4-oxadiazol-2-one derivatives were synthesized and tested for their in vitro antimycobacterial activity. Oxadiazolone derivatives showed an interesting antimycobacterial activity against the tested strain of *Mycobacterium tuberculosis* $H_{37}Rv$, whereas the corresponding thione derivatives were devoid of activity. Molecular modeling investigations showed that the active compounds may interact at the active site of the mycobacterial cytochrome P450-dependent sterol 14α-demethylase in the sterol biosynthesis pathway and that their binding free energy values are in agreement with their MIC values.
© 2005 Elsevier Ltd. All rights reserved.

1. Introduction

The emergence of multidrug resistant strains (MDR) of *Mycobacterium tuberculosis*[1–4] together with the spread of severe opportunistic disseminated infections produced by mycobacteria other than tuberculosis (MOTT), particularly *Mycobacterium avium*[5] in immunocompromised patients prompted the search for new antimycobacterial agents.

Tuberculosis (TB), estimated to infect about one-third of the world's population, still remains the world-wide main cause of death among the infectious disease.

In spite of the availability of effective antitubercular drugs, such as isoniazid and rifampin, the emergence of resistant strains of *M. tuberculosis*, the pathogenic

synergy of the tubercular and nontubercular mycobacterial infections with HIV infections,[5–8] the scarse compliance with the complex therapeutic regimens, justify the effort directed to the design of new drugs for the treatment of tuberculosis and other atypical mycobacterioses. It has been reported[9] that conversion of isoniazid to oxadiazoles produced the corresponding 5-substituted 3*H*-1,3,4-oxadiazol-2-thione and 3*H*-1,3,4,-oxadiazol-2-one and their 3-alkyl or aralkyl derivatives, characterized by antimycobacterial activity against *M. tuberculosis* $H_{37}Rv$.

With the aim to obtain new antimycobacterial agents, we synthesized a series of 5-(pyridin-4-yl)-3*H*-1,3,4-oxadiazol-2-thione **1a–l** and 5-(pyridin-4-yl)-3*H*-1,3,4-oxadiazol-2-one **2a–l** derivatives, in which the nitrogen at the 3 position is linked through a methylene bridge to a cyclic amine. The in vitro antimycobacterial activities of derivatives **1a–l** and **2a–l** were tested against a strain of *M. tuberculosis* $H_{37}Rv$ in comparison with isoniazid and ofloxacin.

Since some of the synthesized compounds showed a remarkable antimycobacterial activity, we made a study in order to verify, through a drug/enzyme complex

[☆] A preliminary account of this work was presented at XVI National Meeting on Medicinal Chemistry, Sorrento, September 18–22, 2002.
* Corresponding author. Tel.: +39 040 574181; fax: +39 040 52572; e-mail: mamolo@units.it

modeling, if their activity may be due to the interaction with the mycobacterial cytochrome P450-dependent sterol 14α-demethylase (P450$_{14DM}$, CYP51) in the sterol biosynthesis pathway.

Actually it was established, using genomic DNA from the *M. tuberculosis* (MT) H$_{37}$Rv strain, that the CYP 51-like gene encodes a bacterial sterol 14α-demethylase (MT P450$_{14DM}$), which acts on 14α-methyl sterols and binds known antifungal azole inhibitors of P450$_{14DM}$.[10]

Targeting MT P450$_{14DM}$ offers a possibility in drug design for new antimycobacterial agents. Here we report the in vitro antimycobacterial activity of compounds **1a–l** and **2a–l** and a molecular modeling study in order to rationalize the possible interactions between the synthesized compounds and the active site of 14DM and verify the agreement between the calculated binding free energy values of compounds and their MIC values.

2. Chemistry

3-Substituted 5-(pyridin-4-yl)-3*H*-1,3,4-oxadiazole-2-thiones **1a–l** (Table 1) were prepared (Scheme 1) by cyclization of isonicotinic acid hydrazide using carbon disulfide in presence of KOH[11] and treatment of the obtained 5-(pyridin-4-yl)-3*H*-1,3,4-oxadiazol-2-thione **1** with formaldehyde and cyclic amines.

The synthesis of the corresponding 3-substituted 5-(pyridin-4-yl)-3*H*-1,3,4-oxadiazol-2-ones **2a–l** (Table 1) was carried out (Scheme 1) by reaction of cyclic amines and formaldehyde with 5-(pyridin-4-yl)-3*H*-1,3,4-oxadiazol-2-one **2**, which in turn was prepared from isonicotinic acid hydrazide and dimethylcarbamyl chloride, according to the previously proposed method.[12]

3. Results and discussion

A series of 1,3,4-oxadiazole-2-thione **1a–l** and 1,3,4-oxadiazol-2-one **2a–l** derivatives have been synthesized with the aim to evaluate their antimycobacterial activity toward a strain of *M. tuberculosis* H$_{37}$Rv sensitive to isoniazid.

The results of the in vitro evaluation of antimycobacterial activity of compounds are reported in Table 2. The oxadiazolone derivatives **2a–l** exhibit an interesting activity against the tested strain, reaching MIC values of 1.25 µg/mL for compounds **2d** and **2f** and 2.5 µg/mL for all other compounds.
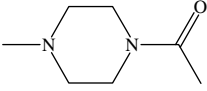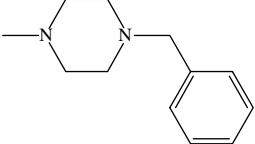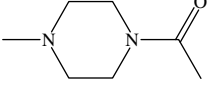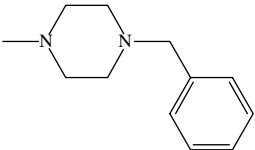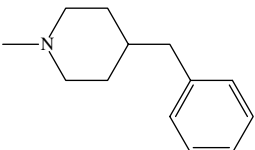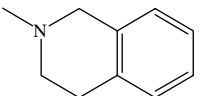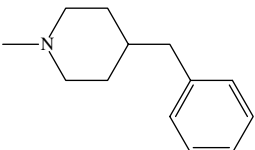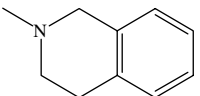
However, the antimycobacterial activity the 1,3,4-oxadiazole-2-thione derivatives **1a–l** is very low or absent. The presence in the active compounds **2a–l** of the carbonyl function seems to be responsible for the greatest potency of these compounds with respect to the corresponding thione derivatives **1a–l**. This consideration and the promising obtained results encourage us to advance in the design, synthesis and evaluation of new modified 1,3,4-oxadiazol-2-one derivatives.

As a result of the applied docking procedure, we obtained a common binding mode for both two series of compounds analyzed in the 14DM active site (see Fig. 1). The active site residues interacting with the inhibitors consisted of helix I, Meander 1, β6–1 (which composes the side of the active site), and β6–2, the C-terminus of helix F, and the β1-5-N-terminus of helix B′, which constitutes the dome of the active site (see Fig. 2). In particular, all hydrophobic substituents find location in a hydrophobic subsite above the heme ring. The residues lining the subsite included the side chains of Q72, A73, A75, Y76, M79, F83, M99, L100, A256,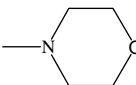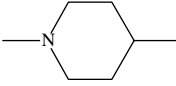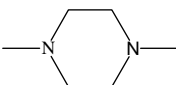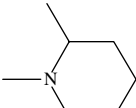 L321, V434, and V435. Interestingly, the 17-alkyl side chain of the substrate lanosterol, the substituted phenyl of azole inhibitors, and newly synthesized nonazole active compounds were also found to be located in this subsite, on the basis of crystal structure and docking analysis.[16–19] The oxadiazolone ring lies parallel to the heme group, just above the iron ion, at an average dynamic distance (ADD) of 5.7 Å, and is favorable encased by the side chains of aminoacids K97, L100, and H101 on one side, and P320, L321, and L324 on the other. The 4-pyridine moiety is nicely encased in another subsite, composed by S148, L152, S252, M253, F255, A256, G257, and T260. Here, the 4-pyridine N of all compounds H-bonds with the NH of the peptide bond between A 256 and G 257, with an average dynamic length (ADL) of 2.89 Å. Further, the ADD between the N atom of this ring and the conserved threonine of helix 1, T260, a residue found involved in the substrate catalytic reaction,[20] is only 4.5 Å.

In a similar fashion to what observed for the invariant OH-group of different lanosterols docked into the protein active site,[21] the double-bonded sulfur and oxygen atoms of the oxadiazolone moiety do not hydrogen bond any of the protein atoms, but are located in the hydrophilic environment of amide nitrogens of I322 and I323. At the same time, however, in the case of all compounds of series **2**, a water molecule forms a duo of hydrogen bonds to the carbonyl oxygen of the oxazolone ring of the inhibitors (ADL = 2.80 Å) and the –OH group of the Y76 side chain (ADL = 2.72 Å).

Deeper and more quantitative information about the forces involved in substrate binding can be obtained by analyzing the values of the free energy of binding, ΔG_{bind} and its components, which are listed in Tables 3 and 4 for the ligands of series **1** and **2**, respectively. For both series of compounds, the intermolecular van der Waals and the electrostatics are both important contribution to the binding. However, the electrostatic desolvation penalty (ΔG_{PB}) offsets the favorable (negative) intermolecular electrostatics, yielding an unfavorable net electrostatic contribution to the binding. Generally speaking, the scaffold 1,3,4-oxadiazole-2-thione does not form any persistent hydrogen bond with the surrounding residues, and the intermolecular electrostatics interactions are accordingly weak. Furthermore, the desolvation penalty upon binding for this series of molecules is quite large; thereby, the net electrostatic contributions to the binding for these inhibitors are significantly unfavorable. On the contrary, for series **2**

Table 1. Yields and physical data of the synthesized compounds

1a-l   **2a-l**

X	Compound	Yield (%)	Mp (°C)	Anal. CHN	Compound	Yield (%)	Mp (°C)	Anal. CHN
	1a	38	100	$C_{14}H_{17}N_5O_2S$	**2a**	65	174–176	$C_{14}H_{17}N_5O_3$
	1b	91	156	$C_{19}H_{21}N_5OS$	**2b**	34	173–175	$C_{19}H_{21}N_5O_2$
	1c[a11,13]	40	115	$C_{13}H_{16}N_4OS$	**2c**[14]	46	168–170	$C_{13}H_{16}N_4O_2$
	1d	46	100	$C_{14}H_{18}N_4OS$	**2d**	34	85	$C_{14}H_{18}N_4O_2$
	1e	39	117	$C_{20}H_{22}N_4OS$	**2e**	25	140	$C_{20}H_{22}N_4O_2$
	1f	43	135	$C_{17}H_{16}N_4OS$	**2f**	36	154	$C_{17}H_{16}N_4O_2$
	1g[a11,13]	41	144	$C_{12}H_{14}N_4O_2S$	**2g**[15]	81	168–169	$C_{12}H_{14}N_4O_3$
	1h	67	125	$C_{14}H_{18}N_4OS$	**2h**	48	144–145	$C_{14}H_{18}N_4O_2$
	1i	38	140	$C_{13}H_{17}N_5OS$	**2i**[15]	41	138–140	$C_{13}H_{17}N_5O_2$
	1j[11]	73	80	$C_{14}H_{18}N_4OS$	**2j**	59	87–90	$C_{14}H_{18}N_4O_2$
	1k[11]	90	87	$C_{14}H_{18}N_4OS$	**2k**	38	65	$C_{14}H_{18}N_4O_2$
	1l	81	158	$C_{12}H_{14}N_4OS_2$	**2l**	35	153–155	$C_{12}H_{14}N_4O_2S$

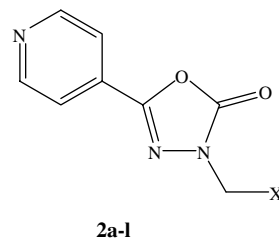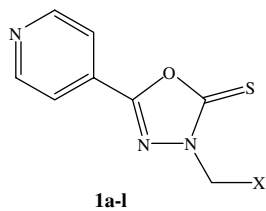[a] These compounds have been described as hydrochlorides.
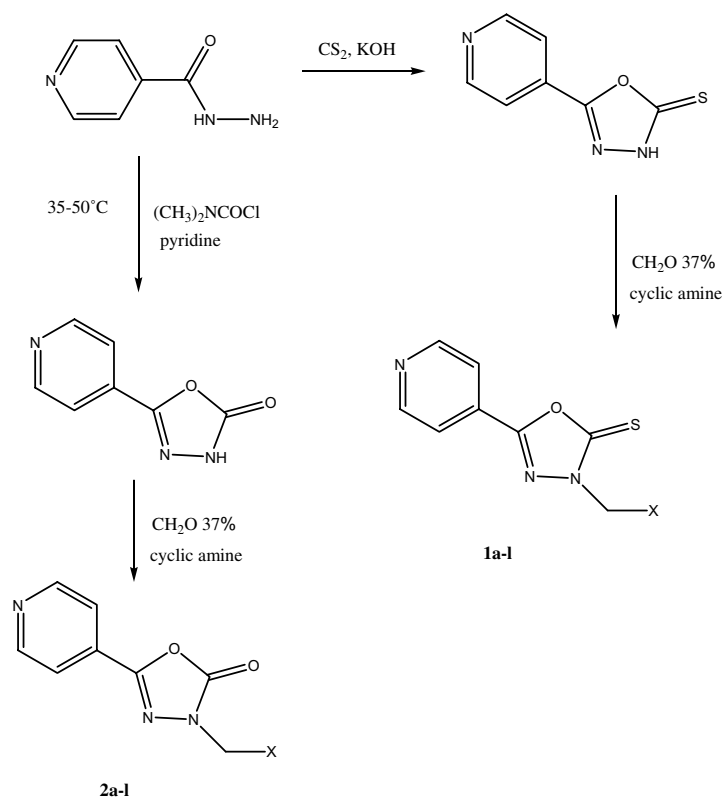
Scheme 1. X = 4acetylpiperidine, *N*-benzylpiperidine, piperidine, 3-methylpiperidine, 4-benzylpiperidine, isoquinoline, morpholine, 4-methylpiperidine, 4-methylpiperazine, 2-methylpiperidine, azepane, thiomorpholine.

inhibitors, despite the somewhat larger unfavorable desolvation energy, in harmony with the larger molecular polarity, the enhanced electrostatic and van der Waals contribution render these molecules tighter binders. In details, the mean value of electrostatic energy ($\Delta E_{ele} + \Delta G_{PB}$) is 29.8 kcal/mol for series **1** and 25.1 kcal/mol for series **2**, with a root-mean-square deviation (RMSD) of 2.0 and 2.1 kcal/mol, respectively. For the van der Waals and hydrophobic interaction energies ($\Delta E_{vdW} + \Delta G_{NP}$), the mean values are −46.3 kcal/mol for series **1** and −47.1 kcal/mol for series **2**, with a root-mean-square deviation of 1.5 and 1.2 kcal/mol, respectively. The calculated changes in solute entropy, $-T\Delta S$, are physically reasonable. The smaller compounds, with their rigid oxadiazolone moiety bound to an aromatic ring reveal the smallest changes in solute entropy upon binding, and this value increases both by increasing the substituent size and by virtue of the presence of the flexible CH_2 joint. More importantly in the framework of computer-assisted drug design, all calculated values for the total free energy of binding are in harmony with the experimentally measured values of the corresponding MIC (see Table 3). In fact, not only series **1** possess consistently lower values of binding affinity with respect of the alternative series **2**, but also there is an excellent agreement in the trend of ΔG_{bind} versus MIC within each series of inhibitors.

As an example, Figures 3 and 4 show the last snapshots of the two most productive binding mode, corresponding to compounds **1d** ($\Delta G_{bind} = -6.1$ kcal/mol) and **2f**

($\Delta G_{bind} = -11.5$ kcal/mol), respectively. Several favorable interactions between the ligands and the enzyme are clearly shown in these Figures: beside the common hydrogen bond between the ligand and the receptor, and, in the case of **2f**, the water-mediated H-bridge discussed above, there are a plethora of favorable van der Waals and hydrophobic interactions that can justify the high affinity for the receptor. In the case of compound **1d**, for instance, the 3-methyl group of the piperidine substituent is in the favorable position of being parallel with the aromatic side chain of Y76, with an average separation of 3.8 Å. Moreover, the side chain methyl groups of L321, Q72, and A73 also make good van der Waals interactions with the hydrocarbonic part of the same heterocycle. Utterly similar considerations can be developed for the analogous compound **2d**, which is ranked as the second best binding inhibitor in series **2**. As concerns compound **2f**, Figure 3 reveals a further, important π–π stabilizing occurring between the condensed ring substituent of **2f** and the phenyl side chain of Y76, resulting from the parallel-displaced geometry of these residues. The electronic nature of the π–π interactions indeed favor the stacking of aromatic rings either by parallel displaced (off-center) or edge-on (*T*-stacking) geometries, while the face-to-face geometry is unfavorable (particularly in environments where there is a low effective dielectric constant), since the dominant interaction is π-electron repulsion. Such a face-to-face situation is encountered, for instance, in compounds **1b,e**, and **2b,e** resulting in a smaller inhibitory efficacy, as testified both by the calculated ΔG_{bind}

Table 2. Activity of compounds **1a–l** and **2a–l** against *M. tuberculosis* H$_{37}$Rv[a]

1a-l　　　　**2a-l**

X	Compound	MIC (µg/mL)	Compound	MIC (µg/mL)
(N-acetylpiperazinylmethyl)	1a	20	2a	2.5
(N-benzylpiperazinylmethyl)	1b	40	2b	2.5
(piperidinylmethyl)	1c	40	2c	2.5
(3-methylpiperidinylmethyl)	1d	10	2d	1.25
(4-benzylpiperidinylmethyl)	1e	40	2e	2.5
(tetrahydroisoquinolinylmethyl)	1f	40	2f	1.25
(morpholinylmethyl)	1g	40	2g	2.5
(4-methylpiperidinylmethyl)	1h	20	2h	2.5
(N-methylpiperazinylmethyl)	1i	40	2i	2.5
(2-methylpiperidinylmethyl)	1j	40	2j	2.5
(azepanylmethyl)	1k	40	2k	2.5
(thiomorpholinylmethyl)	1l	40	2l	2.5

[a] *M. tuberculosis* H$_{37}$Rv strain resulted sensitive to isoniazid (5 µg/disk) and ofloxacin (15 µg/disk).
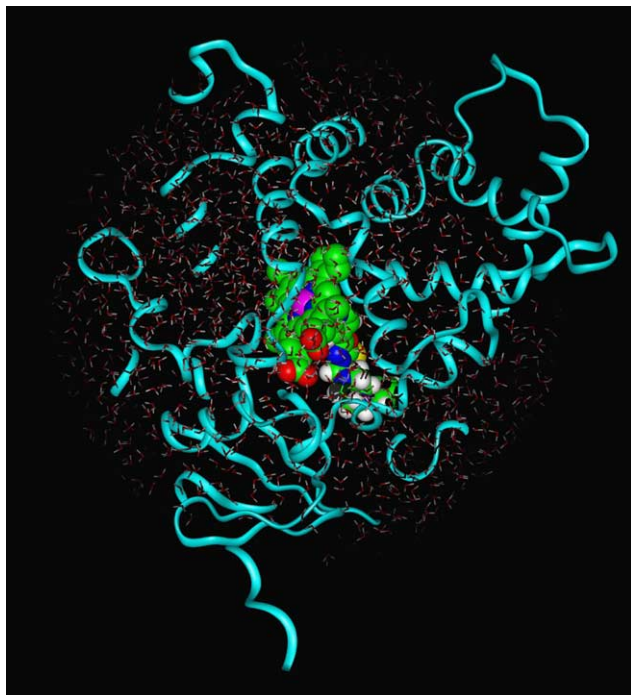
Figure 1. The structure of a 14DM/drug complex. The heme group and the ligand are explicitly shown in CPK representation. The water molecules are shown as lines.

(−2.2 and −3.6 kcal/mol for compounds **1b,e**, and −8.3 and −8.6 for compounds **2b,e**, respectively) and the corresponding MIC values (see Table 4).

4. Conclusions

The application of a combined of docking/MM-PBSA free energy of binding calculations allowed us to rationalize the interactions between the two series of inhibitors and the active site of the 14DM both from a qualitative and most importantly from a quantitative point of view. Particularly in the last case, we verified an agreement between the calculated ΔG_{bind} values of all compounds and the correspondent experimental evidences, expressed in terms of MIC. Accordingly, the models and procedures proposed will be used in the targeted computer-assisted drug design and subsequent prediction of activity of the new, potential inhibitors in reasonable length of computer and human time.

5. Experimental

Melting points were determined with a Buchi 510 capillary apparatus, and are uncorrected. Infrared spectra in Nujol mulls were recorded on a Jasko FT 200 spectrophotometer. Proton nuclear magnetic resonance (^{1}H NMR) spectra were determined on a Varian Gemini 200 spectrometer, chemical shifts are reported as δ (ppm) in CDCl$_3$ solution. Reaction courses and product mixtures were routinely monitored by thin-layer chromatography (TLC) on silica gel precoated F$_{254}$ Merck plates. ESI-MS spectra were obtained on a PE-API I
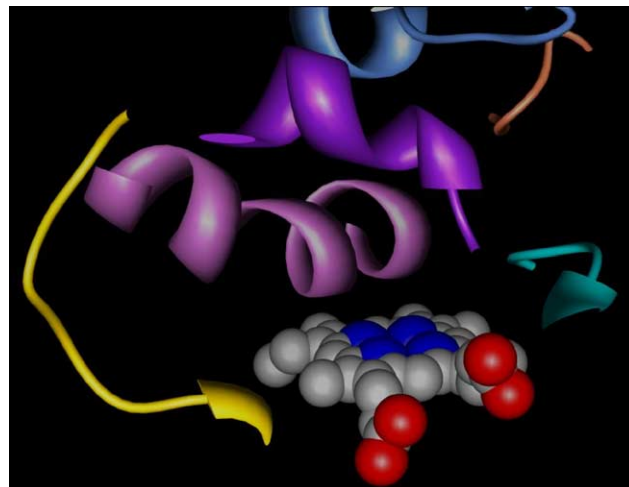

Figure 2. Cartoon of the secondary structural motifs of 14α-sterol demethylase forming the protein active site. β1–5-B′ helix (residues 76–84): purple; meander 1 (residues 87–94): gold; F helix, C-terminus (residues 172–179): cornflower blue; I helix (residues 249–261): orchid; β6–1 sheet (residues 321–326): cyan; β6–2 sheet (residues 431–435): orange. The heme prosthetic group is also shown in atom-colored CPK representation.

spectrometer by infusion of a solution of the sample in MeOH. Elemental analyses (C, H, N) were performed on a Carlo Erba analyzer and were within ±0.3 of the theoretical value.

6. Synthesis

6.1. 3-(4-Acetyl-piperazin-1-ylmethyl)-5-(pyridin-4-yl)-3*H*-1,3,4-oxadiazole-2-thione (1a)

To an suspension of 1 g (5.6 mmol) of 5-(pyridin-4-yl)-3*H*-1,3,4-oxadiazole-2-thione **1** in 30 mL of absolute ethanol, 0.72 g (5.6 mmol) of 1-acetylpiperazine were added. To the stirred suspension 0.45 g (5.6 mmol) of 37% formaldehyde were added dropwise and the reaction mixture was heated under reflux for 24 h. After concentration under reduced pressure, the residue was recrystallized from absolute ethanol affording 1.30 g (73%) of **1a**. Mp 100–102 °C. IR (Nujol, cm^{-1}): 1640, 1123. ^{1}H NMR (CDCl$_3$/TMS): δ 2.05 (s, 3H, CH$_3$), 2.78–2.90 (m, 4H, CH$_2$ pip.), 3.40–3.70 (m, 4H, CH$_2$ pip.), 5.15 (s, 2H, CH$_2$ exocyclic), 7.78 (d, 2H, pyr., J = 5.86 Hz), 8.82 (d, 2H, pyr., J = 5.86 Hz). MS: m/z 320 [MH$^+$]. Anal. Calcd for C$_{14}$H$_{17}$N$_5$O$_2$S (MW 319.38): C, 52.65; H, 5.37; N, 21.93. Found: C, 52.48; H, 5.35; N, 22.07.

6.2. 3-(4-Acetyl-piperazin-1-ylmethyl)-5-(pyridin-4-yl)-3*H*-1,3,4-oxadiazol-2-one (2a)

To an aqueous solution of 1 g (6.1 mmol) of 5-(pyridin-4-yl)-3*H*-1,3,4-oxadiazol-2-one **2**, 0.78 g (6.1 mmol) of 1-acetylpiperazine were added. To the stirred solution 0.5 g (6 mmol) of 37% formaldehyde were added dropwise. After addition, the solution was heated under reflux for 1 h. Thereafter, the reaction mixture was

Table 3. Free energy components and total binding free energies for compounds **1a–l**

	1a	1b	1c	1d	1e	1f	1g	1h	1i	1j	1k	1l
ΔE_{EL}	−19.6	−14.4	−12.9	−15.5	−15.6	−13.1	−14.0	−15.6	−12.7	−11.3	−14.1	−13.7
ΔE_{vdW}	−44.6	−44.7	−39.9	−40.8	−44.9	−44.3	−40.5	−39.8	−40.9	−41.3	−40.6	−40.2
ΔE_{MM}	64.2	−59.1	−52.8	−56.3	−60.5	−57.4	−54.5	−55.4	−53.6	−52.6	−54.7	−53.9
ΔG_{NP}	−4.5	−5.1	−4.1	−4.4	−5.0	−4.6	−4.1	−4.3	−4.3	−4.2	−4.2	−4.1
ΔG_{PB}	50.3	46.8	42.2	42.3	46.1	45.4	44.2	42.1	43.1	42.0	42.5	43.6
ΔG_{sol}	45.8	41.7	38.1	37.9	41.1	40.8	40.1	37.8	38.8	37.8	38.3	39.5
$\Delta G_{MM/PBSA}$	−18.4	−17.4	−14.7	−18.4	−19.4	−16.6	−14.4	−17.6	−14.8	−14.8	−16.4	−14.4
$T\Delta S$	14.3	15.2	12.1	12.3	15.8	12.7	12.0	12.9	12.9	12.6	15.1	12.2
ΔG_{bind}	−4.1	−2.2	−2.6	−6.1	−3.6	−3.9	−2.4	−4.7	−1.9	−2.2	−1.3	−2.2

All values are in kcal/mol.

Table 4. Free energy components and total binding free energies for compounds **2a–l**

	2a	2b	2c	2d	2e	2f	2g	2h	2i	2j	2k	2l
ΔE_{EL}	−28.4	−20.0	−23.0	−23.7	−21.0	−23.4	−22.7	−23.5	−22.8	−22.5	−24.3	−22.1
ΔE_{vdW}	−44.9	−49.0	−40.5	−40.5	−48.2	−45.0	−41.0	−40.1	−41.3	−40.1	−40.6	−40.9
ΔE_{MM}	73.3	−69.0	−63.5	−64.2	−69.2	−68.4	−63.7	−63.6	−64.1	−62.6	−64.9	−63.0
ΔG_{NP}	−4.5	−5.0	−4.1	−4.4	−5.0	−4.5	−4.2	−4.3	−4.4	−4.1	−4.2	−4.1
ΔG_{PB}	54.6	50.7	47.0	46.2	50.5	49.3	47.2	46.5	47.2	45.8	46.2	47.7
ΔG_{sol}	50.1	45.7	42.9	41.8	45.5	44.8	43.0	42.2	42.8	41.7	42.0	43.6
$\Delta G_{MM/PBSA}$	−23.2	−23.3	−20.6	−22.4	−23.7	−23.6	−20.7	−21.4	−21.3	−20.9	−22.9	−19.4
$T\Delta S$	14.8	15.0	12.3	12.1	15.1	12.1	12.3	12.6	12.5	12.8	15.2	12.2
ΔG_{bind}	−8.4	−8.3	−8.3	−10.3	−8.6	−11.5	−8.4	−8.8	−8.8	−8.1	−7.7	−7.2

All values are in kcal/mol.

Figure 3. Equilibrated molecular dynamics snapshot of the docked compound **1d** in the active site of 14α-sterol demethylase. The heme group is shown in atom-colored ball-and-stick, the amino acid in atom-colored stick and the ligand in pink-colored stick representation. For the sake of simplicity, only the amino acids pertaining to the binding site or contacting the ligand are shown. Water molecules and hydrogen atoms are also omitted for clarity.
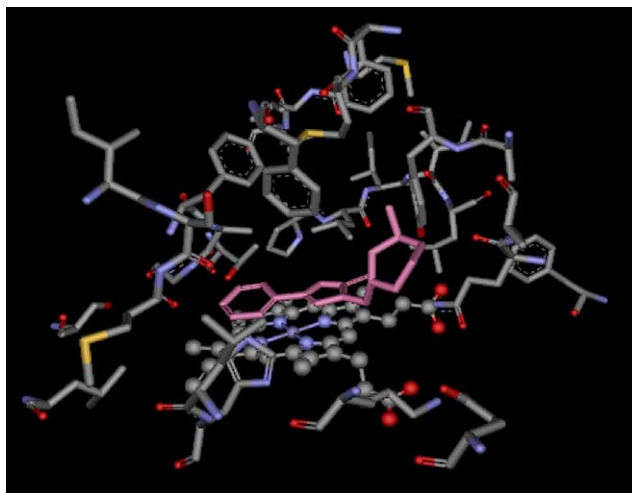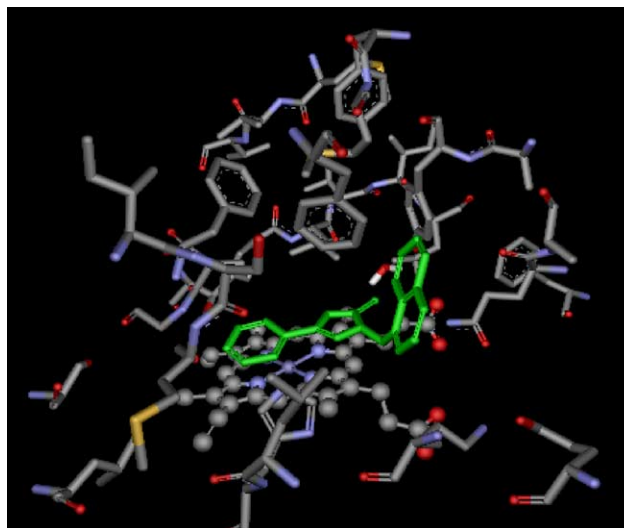

Figure 4. Equilibrated molecular dynamics snapshot of the docked compound **2f** in the active site of 14α-sterol demethylase. The heme group is shown in atom-colored ball-and-stick, the amino acid in atom-colored stick and the ligand in green-colored stick representation. For the sake of simplicity, only the amino acids pertaining to the binding site or contacting the ligand are shown. Only the water molecule forming an H-bridge between **2f** and the protein is shown in color-line representation; hydrogen atoms are also omitted for clarity.

cooled at room temperature and washed repeatedly with chloroform. After washing the organic phase was concentrated under reduced pressure and the precipitate was collected by filtration and recrystallized from ethanol to give 1.2 g (65%) of the white solid. Mp 174–176 °C. IR (Nujol, cm^{-1}): 1770, 1647. ^{1}H NMR (CDCl$_3$/TMS): δ 1.99 (s, 3H, CH$_3$), 2.62–2.75 (m, 4H, CH$_2$ pip.), 3.38–3.62 (m, 4H, CH$_2$ pip.), 4.70 (s, 2H, CH$_2$ exocyclic), 7.62 (d, 2H, pyr., *J* = 6.04 Hz), 8.74 (d, 2H, pyr., *J* = 6.04 Hz). MS: *m/z* 304 [MH$^+$]. Anal. Calcd for C$_{14}$H$_{17}$N$_5$O$_3$ (MW 303.32): C, 55.44; H, 5.65; N, 23.09. Found: C, 55.70; H, 5.45; N, 22.87.

The following compounds **1b–l** and **2b–l** were similarly obtained. Yields and melting points are reported in Table 1.

6.3. 3-(4-Benzyl-piperazin-1-ylmethyl)-5-pyridin-4-yl-3*H*-1,3,4-oxadiazole-2-thione (1b)

IR (Nujol, cm^{-1}): 1150. ^{1}H NMR (CDCl$_3$/TMS): δ 2.40–2.55 (m, 4H, CH$_2$ pip.), 2.80–2.90 (m, 4H, CH$_2$ pip.), 3.46 (s, 2H, –CH$_2$–Ph), 5.07 (s, 2H, CH$_2$ exocyclic), 7.25 (m, 5H arom.), 7.72 (d, 2H, pyr., $J = 6.10$ Hz), 8.76 (d, 2H, pyr., $J = 6.10$ Hz). MS: m/z 368 [MH$^+$]. Anal. Calcd for C$_{19}$H$_{21}$N$_5$OS (MW 367.47): C, 62.10: H, 5.76; N, 19.06. Found: C, 61.95; H, 5.52; N, 19.31.

6.4. 3-(Piperidin-1-ylmethyl)-5-pyridin-4-yl-3*H*-1,3,4-oxadiazole-2-thione (1c)

IR (Nujol, cm^{-1}): 1140. ^{1}H NMR (CDCl$_3$/TMS): δ 1.25–1.66 (m, 6H, CH$_2$ pip., H$_3$, H$_4$, H$_5$), 2.65–2.85 (m, 4H, CH$_2$ pip., H$_2$, H$_6$), 5.05 (s, 2H, CH$_2$ exocyclic), 7.76 (d, 2H, pyr., $J = 5.86$ Hz), 8.78 (d, 2H, pyr., $J = 5.86$ Hz). MS: m/z 277 [MH$^+$]. Anal. Calcd for C$_{13}$H$_{16}$N$_4$OS (MW 276.36): C, 56.50: H, 5.84; N, 20.27. Found: C, 56.73; H, 6.02; N, 20.03.

6.5. 3-(3-Methyl-piperidin-1-ylmethyl)-5-pyridin-4-yl-3*H*-1,3,4-oxadiazole-2-thione (1d)

IR (Nujol, cm^{-1}): 1142. ^{1}H NMR (CDCl$_3$/TMS): δ 0.85 (d, 3H, CH$_3$), 1.40–1.80 (m, 5H, CH$_2$ and CH pip., H$_3$, H$_4$, H$_5$), 2.08–3.15 (m, 4H, CH$_2$ pip., H$_2$, H$_6$), 5.07 (s, 2H, CH$_2$ exocyclic), 7.76 (d, 2H, pyr., $J = 5.86$ Hz), 8.77 (d, 2H, pyr., $J = 5.86$ Hz). MS: m/z 291 [MH$^+$]. Anal. Calcd for C$_{14}$H$_{18}$N$_4$OS (MW 290.38): C, 57.91: H, 6.25; N, 19.29. Found: C, 57.78; H, 6.49; N, 19.56.

6.6. 3-(4-Benzyl-piperidin-1-ylmethyl)-5-pyridin-4-yl-3*H*-1,3,4-oxadiazole-2-thione (1e)

IR (Nujol, cm^{-1}): 1078. ^{1}H NMR (CDCl$_3$/TMS): δ 1.15–1.70 (m, 5H, CH$_2$ and CH pip., H$_3$, H$_4$, H$_5$), 2.35–3.18 (m, 4H, CH$_2$ pip., H$_2$, H$_6$), 2.48 (d, 2H, –CH$_2$–Ph), 5.07 (s, 2H, CH$_2$ exocyclic), 7.06–7.28 (m, 5H, arom.), 7.75 (d, 2H, pyr., $J = 5.86$ Hz), 8.78 (d, 2H, pyr., $J = 5.86$ Hz). MS: m/z 367 [MH$^+$]. Anal. Calcd for C$_{20}$H$_{22}$N$_4$OS (MW 366.48): C, 65.55; H, 6.05; N, 15.29. Found: C, 65.31; H, 5.93; N, 15.48.

6.7. 3-(3,4-Dihydro-1*H*-isoquinolin-2-ylmethyl)-5-pyridin-4-yl-3*H*-1,3,4-oxadiazole-2-thione (1f)

IR (Nujol, cm^{-1}): 1161. ^{1}H NMR (CDCl$_3$/TMS): δ 2.85–3.20 (m, 4H, N–CH$_2$–CH$_2$ isoquin.), 4.05 (s, 2H, N–CH$_2$ isoquin.), 5.26 (s, 2H, CH$_2$ exocyclic), 7.0–7.13 (m, 4H, arom. isoquin.), 7.76 (d, 2H, pyr., $J = 6.10$ Hz), 8.79 (d, 2H, pyr., $J = 6.10$ Hz). MS: m/z 325 [MH$^+$]. Anal. Calcd for C$_{17}$H$_{16}$N$_4$OS (MW 324.40): C, 62.94; H, 4.97; N, 17.27. Found: C, 63.15; H, 4.77; N, 17.45.

6.8. 3-(Morpholin-4-ylmethyl)-5-pyridin-4-yl-3*H*-1,3,4-oxadiazole-2-thione (1g)

IR (Nujol, cm^{-1}): 1160. ^{1}H NMR (CDCl$_3$/TMS): δ 2.70–2.84 (m, 4H, CH$_2$–N–CH$_2$ morph.), 3.54–3.71 (m, 4H, CH$_2$–O–CH$_2$ morph.), 5.0 (s, 2H, CH$_2$ exocyclic), 7.70 (d, 2H, pyr., $J = 5.86$ Hz), 8.75 (d, 2H, pyr., $J = 5.86$ Hz). MS: m/z 279 [MH$^+$]. Anal. Calcd for C$_{12}$H$_{14}$N$_4$O$_4$S (MW 278.33): C, 51.78; H, 5.07; N, 20.13. Found: C, 51.91; H, 5.22; N, 19.97.

6.9. 3-(4-Methyl-piperidin-1-ylmethyl)-5-pyridin-4-yl-3*H*-1,3,4-oxadiazole-2-thione (1h)

IR (Nujol, cm^{-1}): 1172. ^{1}H NMR (CDCl$_3$/TMS): δ 0.87 (d, 3H, CH$_3$), 1.05–1.65 (m, 5H, CH$_2$ and CH pip., H$_3$, H$_4$, H$_5$), 2.35–3.14 (m, 4H, CH$_2$ pip., H$_2$, H$_6$), 5.05 (s, 2H, CH$_2$ exocyclic), 7.75 (d, 2H, pyr., $J = 5.86$ Hz), 8.77 (d, 2H, pyr., $J = 5.86$ Hz). MS: m/z 291 [MH$^+$]. Anal. Calcd for C$_{14}$H$_{18}$N$_4$OS (MW 290.38): C, 57.91: H, 6.25; N, 19.29. Found: C, 57.80; H, 6.42; N, 19.55.

6.10. 3-(4-Methyl-piperazin-1-ylmethyl)-5-pyridin-4-yl-3*H*-1,3,4-oxadiazole-2-thione (1i)

IR (Nujol, cm^{-1}): 1177. ^{1}H NMR (CDCl$_3$/TMS): δ 2.25 (s, 3H, CH$_3$), 2.36–2.50 (m, 4H, CH$_2$ pip.), 2.80–2.95 (m, 4H, CH$_2$ pip.), 5.07 (s, 2H, CH$_2$ exocyclic), 7.73 (d, 2H, pyr., $J = 6.10$ Hz), 8.77 (d, 2H, pyr., $J = 6.10$ Hz). MS: m/z 292 [MH$^+$]. Anal. Calcd for C$_{13}$H$_{17}$N$_5$OS (MW 291.37): C, 53.59: H, 5.88; N, 24.04. Found: C, 53.67; H, 6.03; N, 23.80.

6.11. 3-(2-Methyl-piperidin-1-ylmethyl)-5-pyridin-4-yl-3*H*-1,3,4-oxadiazole-2-thione (1j)

IR (Nujol, cm^{-1}): 1084. ^{1}H NMR (CDCl$_3$/TMS): δ 1.05–1.70 (m, 9H, CH$_3$ and CH$_2$ pip., H$_3$, H$_4$, H$_5$), 2.35–3.15 (m, 3H, CH$_2$ and CH pip., H$_2$, H$_6$), 5.16 (s, 2H, CH$_2$ exocyclic), 7.79 (d, 2H, pyr., $J = 6.10$ Hz), 8.83 (d, 2H, pyr., $J = 6.10$ Hz). MS: m/z 291 [MH$^+$]. Anal. Calcd for C$_{14}$H$_{18}$N$_4$OS (MW 290.38): C, 57.91: H, 6.25; N, 19.29. Found: C, 57.74; H, 6.49; N, 19.56.

6.12. 3-(Azepan-1-ylmethyl)-5-pyridin-4-yl-3*H*-1,3,4-oxadiazole-2-thione (1k)

IR (Nujol, cm^{-1}): 1148. ^{1}H NMR (CDCl$_3$/TMS): δ 1.40–1.84 (m, 8H, CH$_2$ azep., H$_3$, H$_4$, H$_5$, H$_6$), 2.97–3.07 (m, 4H, CH$_2$ azep., H$_2$, H$_7$), 5.19 (s, 2H, CH$_2$ exocyclic), 7.79 (d, 2H, pyr., $J = 5.86$ Hz), 8.79 (d, 2H, pyr., $J = 5.86$ Hz). MS: m/z 291 [MH$^+$]. Anal. Calcd for C$_{14}$H$_{18}$N$_4$OS (MW 290.38): C, 57.91: H, 6.25; N, 19.29. Found: C, 57.79; H, 6.03; N, 19.41.

6.13. 5-(Pyridin-4-yl-3-thiomorpholin-4-ylmethyl)-3*H*-1,3,4-oxadiazole-2-thione (1l)

IR (Nujol, cm^{-1}): 1144. ^{1}H NMR (CDCl$_3$/TMS): δ 2.50–2.80 (m, 4H, CH$_2$–S–CH$_2$ thiomorph.), 2.90–3.25 (m, 4H, CH$_2$–N–CH$_2$ thiomorph.) 5.05 (s, 2H, CH$_2$ exocyclic), 7.76 (d, 2H, pyr., $J = 5.86$ Hz), 8.80 (d, 2H, pyr., $J = 5.86$ Hz). MS: m/z 295 [MH$^+$]. Anal. Calcd for C$_{12}$H$_{14}$N$_4$OS$_2$ (MW 294.40): C, 48.96: H, 4.79; N, 19.03. Found: C, 49.12; H, 4.58; N, 19.22.

6.14. 3-(4-Benzyl-piperazin-1-ylmethyl)-5-pyridin-4-yl-3*H*-1,3,4-oxadiazol-2-one (2b)

IR (Nujol, cm^{-1}): 1771. ^{1}H NMR (CDCl$_3$/TMS): δ 2.40–2.55 (m, 4H, CH$_2$ pip.), 2.70–2.85 (m, 4H, CH$_2$ pip.), 3.47 (s, 2H, CH$_2$–Ph) 4.72 (s, 2H, CH$_2$ exocyclic), 7.25 (m, 5H, arom.), 7.65 (d, 2H, pyr., J = 6.10 Hz), 8.74 (d, 2H, pyr., J = 6.10 Hz). MS: m/z 352 [MH$^+$]. Anal. Calcd for C$_{19}$H$_{21}$N$_5$O$_2$ (MW 351.40): C, 64.94; H, 6.02; N, 19.93. Found: C, 65.02; H, 5.97; N, 20.03.

6.15. 3-(Piperidin-1-ylmethyl)-5-pyridin-4-yl-3*H*-1,3,4-oxadiazol-2-one (2c)

IR (Nujol, cm^{-1}): 1753. ^{1}H NMR (CDCl$_3$/TMS): δ 1.24–1.65 (m, 6H, CH$_2$ pip., H$_3$, H$_4$, H$_5$), 2.60–2.75 (m, 4H, CH$_2$ pip., H$_2$, H$_6$), 4.70 (s, 2H, CH$_2$ exocyclic), 7.68 (d, 2H, pyr., J = 5.86 Hz), 8.75 (d, 2H, pyr., J = 5.86 Hz). MS: m/z 261 [MH$^+$]. Anal. Calcd for C$_{13}$H$_{16}$N$_4$O$_2$ (MW 260.29): C, 59.99: H, 6.20; N, 21.52. Found: C, 59.80; H, 6.50; N, 21.40.

6.16. 3-(3-Methyl-piperidin-1-ylmethyl)-5-pyridin-4-yl-3*H*-1,3,4-oxadiazol-2-one (2d)

IR (Nujol, cm^{-1}): 1790. ^{1}H NMR (CDCl$_3$/TMS): δ 0.81 (d, 3H, CH$_3$), 1.35–1.65 (m, 5H, CH$_2$ and CH pip., H$_3$, H$_4$, H$_5$), 1.80–1.90 (m, 4H, CH$_2$ pip., H$_2$, H$_6$), 4.67 (s, 2H, CH$_2$ exocyclic), 7.67 (d, 2H, pyr., J = 6.04 Hz), 8.75 (d, 2H, CH$_2$ pyr., J = 6.04 Hz). MS: m/z 275 [MH$^+$]. Anal. Calcd for C$_{14}$H$_{18}$N$_4$O$_2$ (MW 274.32): C, 61.30; H, 6.61; N, 20.42. Found: C, 61.00; H, 6.53; N, 20.37.

6.17. 3-(4-Benzyl-piperidin-1-ylmethyl)-5-pyridin-4-yl-3*H*-1,3,4-oxadiazol-2-one (2e)

IR (Nujol, cm^{-1}): 1778. ^{1}H NMR (CDCl$_3$/TMS): δ 1.10–1.80 (m, 5H, CH$_2$ and CH pip., H$_3$, H$_4$, H$_5$), 2.28–3.15 (m, 4H, CH$_2$ pip., H$_2$, H$_6$), 2.50 (d, 2H, CH$_2$–Ph), 4.71 (s, 2H, CH$_2$ exocyclic), 7.0–7.30 (m, 5H, arom.), 7.65 (d, 2H, pyr., J = 6.04 Hz), 8.70 (d, 2H, pyr., J = 6.04 Hz). MS: m/z 351 [MH$^+$]. Anal. Calcd for C$_{20}$H$_{22}$N$_4$O$_2$ (MW 350.41): C, 68.55; H, 6.33; N, 15.99. Found: C, 68.60; H, 6.29; N, 15.70.

6.18. 3-(3,4-Dihydro-1*H*-isoquinolin-2-ylmethyl)-5-pyridin-4-yl-3*H*-1,3,4-oxadiazol-2-one (2f)

IR (Nujol, cm^{-1}): 1771. ^{1}H NMR (CDCl$_3$/TMS): δ 2.85–3.10 (m, 4H, N–CH$_2$–CH$_2$ isoquin.), 3.95 (s, 2H, N–CH$_2$ isoquin.), 4.92 (s, 2H, CH$_2$ exocyclic), 7.02–7.24 (m, 4H, arom. isoquin.), 7.69 (d, 2H, pyr., J = 6.10 Hz), 8.75 (d, 2H, pyr., J = 6.10 Hz). MS: m/z 309 [MH$^+$]. Anal. Calcd for C$_{17}$H$_{16}$N$_4$O$_2$ (MW 308.33): C, 66.22: H, 5.23; N, 18.17. Found: C, 66.15; H, 5.26; N, 18.02.

6.19. 3-(Morpholin-4-ylmethyl)-5-pyridin-4-yl-3*H*-1,3,4-oxadiazol-2-one (2g)

IR (Nujol, cm^{-1}): 1770. ^{1}H NMR (CDCl$_3$/TMS): δ 2.60–2.81 (m, 4H, CH$_2$–N–CH$_2$ morph.), 3.58–3.75 (m, 4H, CH$_2$–O–CH$_2$ morph.), 4.69 (s, 2H, CH$_2$ exocyclic), 7.65 (d, 2H, pyr., J = 5.86 Hz), 8.75 (d, 2H, pyr., J = 5.86 Hz). MS: m/z 263 [MH$^+$]. Anal. Calcd for C$_{12}$H$_{14}$N$_4$O$_3$ (MW 262.26): C, 54.96: H, 5.38; N, 21.36. Found: C,54.60; H, 5.30; N, 21.20.

6.20. 3-(4-Methyl-piperidin-1-ylmethyl)-5-pyridin-4-yl-3*H*-1,3,4-oxadiazol-2-one (2h)

IR (Nujol, cm^{-1}): 1782. ^{1}H NMR (CDCl$_3$/TMS): δ 0.89 (d, 3H, CH$_3$), 1.10–1.68 (m, 5H, CH$_2$ and CH pip., H$_3$, H$_4$, H$_5$), 2.28–3.05 (m, 4H, CH$_2$ pip., H$_2$, H$_6$), 4.70 (s, 2H, CH$_2$ exocyclic), 7.65 (d, 2H, pyr., J = 6.04 Hz), 8.74 (d, 2H, pyr., J = 6.04 Hz). MS: m/z 275 [MH$^+$]. Anal. Calcd for C$_{14}$H$_{18}$N$_4$O$_2$ (MW 274.32): C, 61.30; H, 6.61; N, 20.42. Found: C, 61.52; H, 6.48; N, 20.49.

6.21. 3-(4-Methyl-piperazin-1-ylmethyl)-5-pyridin-4-yl-3*H*-1,3,4-oxadiazol-2-one (2i)

IR (Nujol, cm^{-1}): 1783. ^{1}H NMR (CDCl$_3$/TMS): δ 2.24 (s, 3H, CH$_3$), 2.32–2.55 (m, 4H, CH$_2$ pip.), 2.70–2.87 (m, 4H, CH$_2$ pip.), 4.72 (s, 2H, CH$_2$ exocyclic), 7.65 (d, 2H, pyr., J = 6.10 Hz), 8.74 (d, 2H, pyr., J = 6.10 Hz). MS: m/z 276 [MH$^+$]. Anal. Calcd for C$_{13}$H$_{17}$N$_5$O$_2$ (MW 275.31): C, 56.71; H, 6.22; N, 25.44. Found: C, 56.53; H, 6.19; N, 25.39.

6.22. 3-(2-Methyl-piperidin-1-ylmethyl)-5-pyridin-4-yl-3*H*-1,3,4-oxadiazol-2-one (2j)

IR (Nujol, cm^{-1}): 1780. ^{1}H NMR (CDCl$_3$/TMS): δ 1.05–1.80 (m, 9H, CH$_3$ and CH$_2$ pip., H$_3$, H$_4$, H$_5$), 2.30–3.10 (m, 3H, CH$_2$ and CH pip., H$_2$, H$_6$), 4.80 (s, 2H, CH$_2$ exocyclic), 7.68 (d, 2H, pyr., J = 6.10 Hz), 8.75 (d, 2H, pyr., J = 6.10 Hz). MS: m/z 275 [MH$^+$]. Anal. Calcd for C$_{14}$H$_{18}$N$_4$O$_2$ (MW 274.32): C, 61.30; H, 6.61; N, 20.42. Found: C, 61.51; H, 6.59; N, 20.36.

6.23. 3-(Azepan-1-ylmethyl)-5-pyridin-4-yl-3*H*-1,3,4-oxadiazol-2-one (2k)

IR (Nujol, cm^{-1}): 1781. ^{1}H NMR (CDCl$_3$/TMS): δ 1.35–1.80 (m, 8H, CH$_2$ azep., H$_3$, H$_4$, H$_5$, H$_6$), 2.75–3.05 (m, 4H, CH$_2$ azep., H$_2$, H$_7$), 4.78 (s, 2H, CH$_2$ exocyclic), 7.66 (d, 2H, pyr., J = 6.04 Hz), 8.72 (d, 2H, pyr., J = 6.04 Hz). MS: m/z 275 [MH$^+$]. Anal. Calcd for C$_{14}$H$_{18}$N$_4$O$_2$ (MW 274.32): C, 61.30; H, 6.61; N, 20.42. Found: C, 61.21; H, 6.52; N, 20.48.

6.24. 5-(Pyridin-4-yl-3-thiomorpholin-4-ylmethyl)-3*H*-1,3,4-oxadiazol-2-one (2l)

IR (Nujol, cm^{-1}): 1767. ^{1}H NMR (CDCl$_3$/TMS): δ 2.60–2.73 (m., 4H, CH$_2$–S–CH$_2$ thiomorph.), 2.92–3.08 (m, 4H, CH$_2$–N–CH$_2$ thiomorph.), 4.70 (s, 2H, CH$_2$ exocyclic), 7.67 (d, 2H, pyr., J = 6.04 Hz), 8.75 (d, 2H, pyr., J = 6.04 Hz). MS: m/z 279 [MH$^+$]. Anal. Calcd for C$_{12}$H$_{14}$N$_4$O$_2$S (MW 278.33): C, 51.78; H, 5.07; N, 20.13. Found: C, 51.40; H, 5.00; N, 19.87.

7. Microbiology

Antitubercular activity was evaluated by a new color-based microdilution method MRA[22] on *M. tuberculosis* H37Rv reference strain. Briefly, mycobacterium strain was grown 14 days in complete Middlebrook 7H9 broth, to a bacterial density of $0.5–1 \times 10^4$ cfu/mL. Twofold dilutions of each tested compound were prepared from stock solutions (4 µg/mL dimethylsulfoxide) in 96-well plates in complete 7H9 broth, final compound concentrations being 128–0.125 µg/mL. Each bacterial suspension (20 µL) were added to 180 µL of drug-containing culture medium. The plates were sealed and incubated for 7 days at 37 °C; 5 µL resazurin (Sigma–Aldrich, 10 mg/mL sterile water stock solution) were added per well, coloring blue; plates were allowed to incubate at 37 °C for additional 24 h. Plates were finally read by visual inspection for color change from blue to pink in live mycobacterium-containing wells. MIC was defined as the lowest drug concentration that prevented resazurin color change. Isoniazid or rifampicin was always included as positive control in each experiment; each evaluation was performed in triplicate in duplicate experiments. Dimethylsulfoxide has been also evaluated and was always devoided of inhibiting activity up to the concentration of 2% (v/v).

8. Molecular modeling

All calculations were carried out on a cluster of Silicon Graphics Octane R12K computers. The starting point of our simulations was the X-ray structure of cytochrome P450 14α-sterol demethylase (14DM) from *Mycobacterium* in complex with 4-phenylimidazole (PDB entry code 1E9X).[18] Hydrogens were added to the protein backbone and side chains with the PARSE module of the AMBER 6.0 package.[23,24] All ionizable residues were considered in the standard ionization state at neutral pH. The PARM94 version[25] of the all-atom AMBER force field was applied for protein relaxation, with the heme model parameters of Paulsen and Ornstein.[26] The primary cut-off distance for nonbonded interaction was set to 12 Å, the cut-off taper for the Coulomb and van der Waals interactions were 1.2 and 2, respectively. The GB/SA continuum solvation model[27,28] was used to mimic a water environment. Geometry refinement was carried out using the SANDER module via a combined steepest descent—conjugate gradient algorithm, using as a convergence criterion for the energy gradient the root-mean-square of the Cartesian elements of the gradient equal to 0.01 kcal/(mol Å). As expected, no relevant structural changes were observed between the active site of the 14DM relaxed structure and the original 3-D structure.

The model structures of compounds **1a–l** and **2a–l** were generated using the Biopolymer module of INSIGHT II.[29] All molecules were subjected to an initial energy minimization, again using the SANDER module of the AMBER 6.0[23,24] suite of programs, with the PARM94 version[25] of the AMBER force field. In this case, the convergence criterion was set to 10^{-4} kcal/(mol Å). A conformational search was carried out using a well-validated combined molecular mechanics/molecular dynamics simulated annealing (MDSA) protocol.[16,30–32] Accordingly, the relaxed structures were subjected to five repeated temperature cycles (from 298 to 1000 K and back) using constant volume/constant temperature (NVT) MD conditions. At the end of each annealing cycle, the structures were again energy minimized to converge below 10^{-4} kcal/(mol Å), and only the structures corresponding to the minimum energy were used for further modeling. The atomic partial charges for the geometrically optimized compounds were obtained using the RESP procedure,[33,34] and the electrostatic potentials were produced by single-point quantum mechanical calculations at the Hartree–Fock level with a 6–31G* basis set, using the Merz–Singh–Kollman van der Waals parameters.[35,36]

The optimized structures of the antimycobacterial compounds were docked into the 14DM active site according to a validated procedure,[16,31,37] accordingly, it will be described here only briefly. The software AUTODOCK 3.0[38] was employed to estimate the possible binding orientations of all compounds in the receptor. In order to encase a reasonable region of the protein surface and interior volume, centered on the crystallographic identified binding site, the grids were 60 Å on each side. Grid spacing (0.375 Å), and 120 grid points were applied in each Cartesian direction so as to calculate mass-centered grid maps. Amber 12–6 and 12–10 Lennard–Jones parameters were used in modeling van der Waals interactions and hydrogen bonding (N–H, O–H, and S–H), respectively. In the generation of the electrostatic grid maps, the distance dependent relative permittivity of Mehler and Solmajer[39] was applied.

For the docking of each compound to the protein, three hundred Monte Carlo/Simulated Annealing (MC/SA) runs were performed, with 100 constant temperature cycles for simulated annealing. For these calculations, the GB/SA implicit water model[27,28] was again used to mimic the solvated environment. The rotation of the angles ϕ and φ, and the angles of side chains were set free during the calculations. All other parameters of the MC/SA algorithm were kept as default. Following the docking procedure, all structures of compounds **1a–l** and **2a–l** were subjected to cluster analysis with a tolerance of 1 Å for an all-atom root-mean-square (RMS) deviation from a lower-energy structure representing each cluster family. In the absence of any relevant crystallographic information, the structure of each resulting complex characterized by the lowest interaction energy was selected for further evaluation.

Each best substrate/14DM complex resulting from the automated docking procedure was further refined in the AMBER suite using the quenched molecular dynamics method (QMD).[40] In this case, 100 ps MD simulation at 298 K were employed to sample the conformational space of the substrate–enzyme complex in the GB/SA continuum solvation environment.[27,28] The integration step was equal to 1 fs. After each picoseconds, the system was cooled to 0 K, the structure was extensively

minimized, and stored. To prevent global conformational changes of the enzyme, the backbone of the protein binding site were constrained by a harmonic force constant of 100 kcal/Å, whereas the amino acid side chains and the ligands were allowed moving without any constraint.

The best energy configuration of each complex resulting from the previous step was solvated by adding a sphere of TIP3P water molecules[41] with a 30 Å radius from the mass center of the ligand with the use of the cap option of the LEAP module of AMBER 6.0 (see Fig. 1). The protein complex was neutralized adding a suitable number of counterions (Na$^+$ and Cl$^-$) in the positions of largest electrostatic potential, as determined by the module CION of the AMBER 6.0 platform. The counterions, which had distances larger than 25 Å from the active site, were fixed in space during all simulations to avoid artifactual long range electrostatic effects on the calculated free energies. After energy minimization of the water molecules for 1500 steps, and MD equilibration of the water sphere with fixed solute for 20 ps, further unfavorable interactions within the structures were relieved by progressively smaller positional restraints on the solute (from 25 to 0 kcal/(mol Å^2) for a total of 4000 steps. Each system was gradually heated to 298 K in three intervals, allowing a 5 ps interval per each 100 K, and then equilibrated for 50 ps at 298 K, followed by 400 ps of data collection runs, necessary for the estimation of the free energy of binding (vide infra). After the first 20 ps of MD equilibration, additional TIP3P water molecules were added to the 30 Å water cap to compensate for those who were able to diffuse into gaps of the enzyme. The MD simulations were performed at 298 K using the Berendsen coupling algorithm,[42] an integration time step of 2 fs, and the applications of the SHAKE algorithm[43] to constrain all bonds to their equilibrium values, thus removing high frequency vibrations. Long-range nonbonded interactions were truncated by using a 30 Å residue-based cut-off.

For the calculation of the binding free energy between 14DM and compounds **1a–l** and **2a–l** in water, a total of 400 snapshots were saved during the MD data collection period described above, one snapshot per each 1 ps of MD simulation. The binding free energy ΔG_{bind} of each complex in water was calculated according to the procedure termed MM/PBSA (Molecular Mechanic/ Poisson–Boltzmann Surface Area) and proposed by Srinivasan et al.[44] Since the theoretical background of this methodology is described in details in the original papers by Peter Kollman and his group,[45] and the detailed application to 14DM/inhibitor complexes has already been reported in our previous paper,[16] it will be only briefly described below.

Basically, an MD simulation (typically in explicit solvent) is first carried out which yields a representative ensemble of structures. The average total free energy of the system, G, is then evaluated as:

$$G = G_{PB} + G_{NP} + E_{MM} - TS_{solute} \qquad (1)$$

in which G_{PB} is the polar solvation energy component, which is calculated in a continuum solvent, usually a finite-difference Poisson–Boltzmann (PB) model, and G_{NP} is the nonpolar contribution to the solvation energy, which can be obtained from the solvent accessible surface area (SA). E_{MM} denotes the sum of molecular mechanics (MM) energies of the molecule, and can be further split into contributions from electrostatic (E_{EL}), van der Waals (E_{VDW}), and internal (E_{INT}) energies:

$$E_{MM} = E_{EL} + E_{VDW} + E_{INT} \qquad (2)$$

The last term in Eq. 1, TS_{solute} represents the solute entropy, and is usually estimated by a combination of classical statistical formulas and normal mode analysis.

Using Eqs. 1 and 2, the binding free energy ΔG_{bind} of a given noncovalent association can be obtained as:

$$\Delta G_{bind} = G_{complex} - (G_{protein} + G_{ligand}) \qquad (3)$$

The ensemble of structures for the uncomplexed reactants are generated either running separate MD simulations for them or by using the trajectory of the complex, simply removing the atoms of the protein or ligand. As reported below, in this work we follow the successful approach proposed by Kuhn and Kollman,[46] and apply the latter variant. Accordingly, the term E_{INT} in Eq. 2 cancels in the calculations of the free energy of binding. The Poisson–Boltzmann (PB) calculations were done with the DELPHI package,[47] using PARSE atomic radii[48] and Cornell et al. charges,[25] with interior and exterior dielectric constants equal to 1 and 80, respectively. A grid spacing of 2/Å, extending 20% beyond the dimensions of the solute, was employed. The nonpolar component G_{NP} was obtained using the following relationship:[48] $G_{np} = \gamma SA + b$, in which $\gamma = 0.00542$ kcal/(mol Å^2), $b = 0.92$ kcal/mol, and the surface area was estimated by means of the MSMS software.[49]

There are several approaches to estimate the last parameter, that is, the change in solute entropy upon association $-T\Delta S$, including the normal-mode analysis,[50] the quasi-harmonic analysis,[51,52] and the quasi-Gaussian approach.[53] Considering that normal mode has been successfully applied in estimating the binding entropy for several biological systems,[54] in this study the conformational entropies were calculated through normal-mode analysis. In the first step of this calculation, an 8 Å sphere around the ligand was cut out from an MD snapshot for each ligand–protein complex. This value was shown to be large enough to yield converged mean changes in solute entropy. On the basis of the size-reduced snapshots of the complex, we generated structures of the uncomplexed reactants by removing the atoms of the protein and ligand, respectively. Each of those structures was minimized, using a distance-dependent dielectric constant $\varepsilon = 4r$, to account for solvent screening, and its entropy was calculated using classical statistical formulas and normal mode analysis. To minimize the effects due to different conformations adopted by individual snapshots we averaged the estimation of entropy over 10 snapshots and reported

the standard error of the mean as a measure of the variance.

Acknowledgements

References and notes

1. Morris, S.; Bai, G. H.; Suffys, P.; Portilo-Gomez, L.; Fairchok, M.; Rouse, D. *J. Infect. Dis.* **1995**, *171*, 954–960.
2. Telzak, E. E.; Sepkowitz, K.; Alpert, P.; Mannheimer, S.; Mederd, F.; El-Sadr, W.; Blum, S.; Gagliardi, A.; Salomon, N.; Turett, G. *N. Engl. J. Med.* **1995**, *333*, 907–911.
3. Basso, L. A.; Blanchard, J. S. *Adv. Exp. Med. Biol.* **1998**, *456*, 115.
4. Bastian, I.; Colebuuders, R. *Drugs* **1999**, *58*, 633.
5. Inderlied, C. B.; Kemper, C. A.; Bermudez, L. E. M. *Clin. Microbiol. Rev.* **1993**, *6*, 266.
6. Collins, F. M. *Clin. Microbiol. Rev.* **1989**, *2*, 360.
7. Graham, N. M. W.; Galai, N.; Nelson, K. E.; Astemborski, J.; Bonds, M.; Rizzo, R. T.; Sheeley, L.; Vlahov, D. *Arch. Int. Med.* **1996**, *156*, 889.
8. Halsey, N. A.; Coberly, J. S.; Desormeaux, J.; Losikoff, P.; Atkinson, J.; Moulton, L. H.; Contave, M.; Johnson, M.; Davis, H.; Geiter, L.; Johnson, E.; Huebner, R.; Boulos, R.; Chaisson, R. E. *Lancet* **1988**, *351*, 786.
9. Wilder Smith, A. E. *Arzneim. Forsch.* **1966**, *16*, 1034–1038.
10. Bellamine, A.; Mangla, A. T.; Nes, W. D.; Waterman, M. R. *Proc. Natl. Acad. Sci. U.S.A.* **1999**, *96*, 8937–8942.
11. Singh, I. P.; Saxena, A. K.; Shankar, K. *Eur. J. Med. Chem.* **1986**, *21*, 267–270.
12. Yale, H. L.; Losee, A.; Perry, F. M.; Bernstein, J. *J. Am. Chem. Soc.* **1954**, *76*, 2208–2210.
13. Ruravicius, A.; Kuodis, Z. *Heterocycl. Compd.* **2002**, *38*, 852–858.
14. Dornow, A.; Lupfert, S. *Arch. Pharm.* **1955**, *288*, 311–315.
15. Caldwell, H. C.; Seiwald, R. J.; Burckhalter, J. H. *J. Am. Pharm. Assoc.* **1958**, *47*, 799–802.
16. Mamolo, M. G.; Zampieri, D.; Falagiani, V.; Vio, L.; Fermeglia, M.; Ferrone, M.; Pricl, S.; Banfi, E.; Scialino, G. *ARKIVOC* **2004**, *5*, 231.
17. Ji, H.; Zhang, W.; Zhou, Y.; Zhang, M.; Zhu, J.; Song, Y.; Lü, J.; Zhu, J. *J. Med. Chem.* **2000**, *43*, 2493.
18. Podust, L. M.; Poulos, T. L.; Waterman, M. R. *Proc. Natl. Acad. Sci. U.S.A.* **2001**, *98*, 3068.
19. Ji, H.; Zhang, W.; Zhang, M.; Kudo, M.; Aoyama, Y.; Yoshida, Y.; Sheng, C.; Song, Y.; Yang, S.; Zhou, Y.; Lü, J.; Zhu, J. *J. Med. Chem.* **2003**, *46*, 474.
20. Schlichting, I.; Berebdzen, J.; Chu, K.; Srock, A. M.; Maves, S. A.; Benson, D. E.; Sweet, R. M.; Ringe, D.; Petsko, G. A.; Sligar, S. G. *Science* **2000**, *287*, 1615.
21. Podust, L.; Stojan, J.; Poulos, T. L.; Waterman, M. R. Substrate recognition sites in 14a-sterol demethylase from comparative analysis of amino acid sequences and X-ray structure of *Mycobacterium tuberculosis* CYP51. *J. Inorg. Biochem.* **2001**, *87*, 227–235.
22. Banfi, E.; Scialino, G.; Monti-Bragadin, C. *J. Antimicro. Chemother.* **2003**, *52*, 796.
23. Case, D. A.; Pearlman, D. A.; Caldwell, J. W.; Cheatham, T. E., III; Ross, W. S.; Simmerling, C. L.; Darden, T. A.; Merz, K. M.; Stanton, R. V.; Cheng, A. L.; Vincent, J. J.; Crowley, M.; Tsui, V.; Radmer, R. J.; Duan, Y.; Pitera, J.; Massova, I.; Seibel, G. L.; Singh, U. C.; Weiner, P. K.; Kollman, P. A. *AMBER 6*; University of California: San Francisco, USA, 1999.
24. Pearlman, D. A.; Case, D. A.; Caldwell, J. W.; Ross, W. S., III; Cheatham, T. E., III; DeBolt, S.; Ferguson, D.; Seibel, G. L.; Kollman, P. A. *Comp. Phys. Commun.* **1995**, *91*, 1.
25. Cornell, W. D.; Cieplak, P.; Bayly, C. I.; Gould, I. R.; Merz, K. M., Jr.; Ferguson, D. M.; Spellmeyer, D. C.; Fox, T.; Caldwell, J. W.; Kollman, P. A. *J. Am. Chem. Soc.* **1995**, *117*, 5179.
26. Paulsen, M. D.; Ornstein, R. L. A 175-psec molecular dynamics simulation of camphor-bound cytochrome P-450cam. *Proteins: Struct. Funct. Genet.* **1991**, *11*, 184–204.
27. Jayaram, B.; Sprous, D.; Beveridge, D. L. *J. Phys. Chem. B* **1998**, *102*, 9571.
28. Weiser, J.; Shenkin, P. S.; Still, W. C. *J. Comp. Chem.* **1999**, *20*, 217.
29. Insight II Program Package (2000.1), Accelrys Inc., San Diego, CA, USA.
30. Fermeglia, M.; Ferrone, M.; Pricl, S. *Bioorg. Med. Chem.* **2002**, *10*, 2471.
31. Felluga, F.; Pitacco, G.; Valentin, E.; Coslanich, A.; Fermeglia, M.; Ferrone, M.; Pricl, S. *Tetrahedron: Asymmetry* **2003**, *14*, 3385.
32. Manfredini, S.; Solaroli, N.; Angusti, A.; Nalin, F.; Durini, E.; Vertuani, S.; Pricl, S.; Ferrone, M.; Spadari, S.; Focher, F.; Verri, A.; De Clercq, E.; Balzarini, J. *Antivir. Chem. Chemother.* **2003**, *14*, 183.
33. Bayly, C. I.; Cieplak, P.; Cornell, W. D.; Kollman, P. A. *J. Phys. Chem.* **1993**, *97*, 10269.
34. Fox, T.; Kollman, P. A. *J. Phys. Chem. B* **1998**, *102*, 8070.
35. Besler, B. H.; Merz, K. M.; Kollman, P. A. *J. Comput. Chem.* **1990**, *11*, 431.
36. Singh, U. C.; Kollman, P. A. *J. Comput. Chem.* **1984**, *5*, 129.
37. Felluga, F.; Fermeglia, M.; Ferrone, M.; Pitacco, G.; Pricl, S.; Valentin, E. *Tetrahedron: Asymmetry* **2002**, *13*, 475.
38. Morris, G. M.; Goodsell, D. S.; Halliday, R. S.; Huey, R.; Hart, W. E.; Belew, R. K.; Olson, A. J. *J. Comput. Chem.* **1998**, *19*, 1639.
39. Mehler, E. L.; Solmajer, T. *Protein Eng.* **1991**, *4*, 903.
40. Frecer, V.; Kabelac, M.; De Nardi, P.; Pricl, S.; Miertus, S. *J. Mol. Graph. Model* **2004**, *22*, 209.
41. Jorgensen, W. L.; Chandrasekhar, J.; Madura, J. D.; Impey, R. W.; Klein, M. L. *J. Comput. Phys.* **1983**, *79*, 926.
42. Berendsen, H. J. C.; Postma, J. P. M.; van Gunsteren, W. F.; DiNola, A.; Haak, J. R. *J. Comput. Phys.* **1984**, *81*, 3684.
43. Ryckaert, J. P.; Ciccotti, G.; Berendsen, H. J. C. *J. Comput. Phys.* **1977**, *23*, 327.
44. Srinivasan, J.; Cheatham, T. E., III; Cieplak, P.; Kollman, P. A.; Case, D. A. *J. Am. Chem. Soc.* **1998**, *120*, 9401.
45. See, for a good review: Kollman, P. A.; Massova, I.; Reyes, C.; Kuhn, B.; Huo, S.; Chong, L.; Lee, M.; Lee, T.; Duan, Y.; Wang, W.; Donini, O.; Cieplak, P.; Srinivasan, J.; Case, D.; Cheatham, T. E., III. *Acc. Chem. Res.* **2000**, *33*, 889.
46. Kuhn, B.; Kollman, P. A. *J. Med. Chem.* **2000**, *43*, 3786.
47. Gilson, M. K.; Sharp, K. A.; Honig, B. H. *J. Comput. Chem.* **1987**, *9*, 327.
48. Sitkoff, D.; Sharp, K. A.; Honig, B. H. *J. Phys. Chem.* **1994**, *98*, 1978.
49. Sanner, M. F.; Olson, A. J.; Spehner, J. C. *Biopolymers* **1996**, *38*, 305.
50. Wilson, E. B.; Decius, J. C.; Cross, P. C. *Molecular Vibrations*; McGraw-Hill: New York, 1955.

M. G. Mamolo et al. / Bioorg. Med. Chem. 13 (2005) 3797–3809

3809

51. Brooks, B. R.; Janežič, D.; Karplus, M. *J. Comput. Chem.* **1995**, *16*, 1522.

52. Janežič, D.; Brooks, B. R. *J. Comput. Chem.* **1995**, *16*, 1543.

53. Roccatano, D.; Amadei, A.; Apol, M. E. F.; Nola, A. D.; Berendsen, H. J. C. *J. Chem. Phys.* **1998**, *109*, 6358.

54. See for instance: (a) Chong, L. T.; Duan, Y.; Wang, I.; Massova, I.; Kollman, P. A. *Proc. Natl. Acad. Sci. U.S.A.* **1999**, *96*, 14330; (b) Massova, I.; Kollman, P. A. *J. Am. Chem. Soc.* **1999**, *121*, 8133; (c) Wang, J.; Morin, P.; Wang, W.; Kollman, P. A. *J. Am. Chem. Soc.* **2001**, *123*, 5221; (d) Minehardt, T. J.; Marzari, N.; Cooke, R.; Pate, E.; Kollman, P. A.; Car, R. *Biophys. J.* **2002**, *82*, 660; (e) Gouda, H.; Kuntz, I. D.; Case, D. A.; Kollman, P. A. *Biopolymers* **2003**, *68*, 16; (f) Fermeglia, M.; Ferrone, M.; Lodi, A.; Pricl, S. *Carbohydr. Polym.* **2003**, *12*, 2341.